



Thermal conductivity vs depth profiling using the hot disk technique-Analysis of anisotropic, inhomogeneous structures

Downloaded from: <https://research.chalmers.se>, 2024-04-20 11:10 UTC







Citation for the original published paper (version of record):

Sizov, A., Mekonnen Mihiretie, B., Ma, Y. et al (2023). Thermal conductivity vs depth profiling using the hot disk technique-Analysis of anisotropic, inhomogeneous structures. *Review of Scientific Instruments*, 94(7).
<http://dx.doi.org/10.1063/5.0145902>

N.B. When citing this work, cite the original published paper.

RESEARCH ARTICLE | JULY 06 2023

Thermal conductivity vs depth profiling using the hot disk technique—Analysis of anisotropic, inhomogeneous structures

A. Sizov ; B. Mihiretie ; Y. Ma ; S. E. Gustafsson ; M. Gustavsson  



Rev Sci Instrum 94, 074902 (2023)

<https://doi.org/10.1063/5.0145902>



View
Online



Export
Citation

CrossMark

Thermal conductivity vs depth profiling using the hot disk technique—Analysis of anisotropic, inhomogeneous structures

Cite as: *Rev. Sci. Instrum.* **94**, 074902 (2023); doi: [10.1063/5.0145902](https://doi.org/10.1063/5.0145902)

Submitted: 8 February 2023 • Accepted: 22 May 2023 •

Published Online: 6 July 2023



View Online



Export Citation



CrossMark

A. Sizov,¹  B. Mihiretie,²  Y. Ma,²  S. E. Gustafsson,³  and M. Gustavsson^{2,a)} 

AFFILIATIONS

¹Department of Chemistry and Chemical Engineering, Chalmers University of Technology, SE-412 96 Göteborg, Sweden

²Hot Disk AB, Johanneberg Science Park, Sven Hultins gata 9A, Göteborg, Sweden

³Thermetrol AB, Johanneberg Science Park, Sven Hultins gata 9A, Göteborg, Sweden

^{a)}Author to whom correspondence should be addressed: mattias.gustavsson@hotdiskinstruments.com

ABSTRACT

A recently developed method for analyzing the thermal conductivity vs depth variation near a sample surface has been extended to include inhomogeneous samples with anisotropy. If not considered, the anisotropy ratio in the sample structure can distort the depth-position data of the original test method. The anisotropy ratio is introduced in the original computational scheme in order to improve the depth-position estimations for inhomogeneous structures with anisotropy. The proposed approach has been tested in experiments and shown to improve depth position mapping.

© 2023 Author(s). All article content, except where otherwise noted, is licensed under a Creative Commons Attribution (CC BY) license (<http://creativecommons.org/licenses/by/4.0/>). <https://doi.org/10.1063/5.0145902>

I. INTRODUCTION AND THEORETICAL BACKGROUND

A. Homogeneous materials

Transient measurement of thermal conductivity and thermal diffusivity of homogeneous materials utilizing hot disk probes has become a fairly common method used by multiple laboratories.^{1–5} The described method involves utilizing a flat sensor that functions both as a heat source and as a temperature sensor. This sensor is placed between two portions of the sample being examined. An electrical current is then passed through the sensor, causing it to increase its temperature. The temperature response of the sensor is then measured and analyzed to determine the thermal transport properties of the sample. This is achieved by fitting the data to a theoretical model that includes a “shape function.”⁶ The short time approximate solution of the 3D shape function (e.g., $t_{\max} < 0.1\theta$)⁷ closely resembles the corresponding 1D shape function, making it relevant to study variations in thermal conductivity in the through-plane direction.

When testing a sample, an important concept to consider is the thermal depth of probing, or “probing depth,”⁶ which can be assumed to be $d_p = 2\sqrt{a \cdot t}$. Here, a is the thermal diffusivity of the sample and t is the time measured from the start of the experiment.

Factor 2 represents an empirical finding for the present experimental setup (the number 2 depends on the measurement sensitivity of the experimental apparatus).⁶ This concept of probing depth is used to visualize the geometrical zone in the sample—around the probe—where temperature increases in a way that has a measurable impact on the temperature vs time data recorded by the probe itself.

B. Inhomogeneous materials

1. Geometry assumption in initial computational scheme

In an earlier paper,⁷ an attempt was made to estimate the thermal conductivity variation vs depth by considering a single experiment, tested with a single sensor, at only one surface position. In this scenario, a short time window within the total temperature–time transient curve was analyzed. By assuming a constant specific heat value across the entire inhomogeneous structure (which is a rather accurate assumption for most dense inert materials),⁸ it was experimentally and theoretically demonstrated that the slope of the time window would more or less weakly connect with the local thermal conductivity at a certain depth position, while simultaneously the

estimated depth position of this local thermal conductivity would be more or less accurately estimated.

Some examples provided in Ref. 9 demonstrate the ability—as well as the limitations—of this testing approach. The following characteristics were found:

- Thermal conductivity vs depth profiles were highly reproducible.
- The method was suitable for the analysis of dense structures [as the volumetric specific heat is theoretically (via the theory of solid-state physics) shown always to be within $\sim 1-4 \frac{\text{MJ}}{\text{m}^3 \text{K}}$ for all dense, inert materials at room temperature conditions].⁸
- For situations in which the assumed volumetric specific heat value was incorrectly set, an overall shift in the thermal conductivity vs depth slope was obtained in the computations—resulting also in an overall shifting of the depth positions toward increased errors.

2. Sensor selection and anisotropy ratio (AR)

The same guidelines on devising an experiment as presented in Ref. 7 are also valid here—with the additional consideration of an underlying anisotropy. The selection of sensor size presented in Ref. 7 was stated as follows for an inhomogeneous isotropic structure: the total test time t_{max} is recommended to be selected significantly shorter than the average “characteristic” time of the sensor ($\theta = \frac{r^2}{a_{\text{av},\text{in-plane}}}$, where r is the radius of the hot disk sensor), e.g., $t_{\text{max}} < 0.1\theta$. In this situation, the 3D shape function presents almost the same output as the corresponding 1D shape function. That is, for such short-time tests, the sensor mainly detects the thermal conductivity variation in the normal direction of the sensor plane and is, hence, the recommended selection of test time for the inhomogeneity variation computations.

However, in a situation where an underlying anisotropy exists, the proposed measurement approach requires knowledge of the true volumetric specific heat value $(\rho c_p)_{\text{true}}$, as well as the anisotropy ratio AR —of which both are assumed to be constant throughout the sample.

In case the anisotropy ratio is not known, a hot disk standard measurement can be performed to determine AR , however using a significantly longer time window than that used in the following inhomogeneity computations: When conducting a regular hot disk experiment with a measurement time falling within the recommended range of $0.33 < t_{\text{max}}/\theta < 1$,¹⁰ using the estimated thermal conductivity $\sqrt{\lambda_{\text{in-plane}}\lambda_{\text{through-plane}}}$ and estimated thermal diffusivity ($a_{\text{in-plane}}$), the false volumetric specific heat value $(\rho c_p)_{\text{false}}$ can be computed as

$$(\rho c_p)_{\text{false}} = \frac{\sqrt{\lambda_{\text{in-plane}}\lambda_{\text{through-plane}}}}{a_{\text{in-plane}}}. \quad (1)$$

Given the knowledge of the true volumetric specific heat $(\rho c_p)_{\text{true}}$, the anisotropy ratio AR can be estimated by rearranging Eq. (1) as follows:

$$(\rho c_p)_{\text{false}} = (\rho c_p)_{\text{true}} \cdot \frac{1}{\sqrt{AR}}. \quad (2)$$

II. COMPUTATIONS

For an anisotropic sample, the false volumetric specific heat value $(\rho c_p)_{\text{false}}$ is used for the iterative computations described in Ref. 7 (replacing the true volumetric specific heat). From this, it can be mathematically shown that the iterative computations will render the following estimations (assuming the AR ratio is constant throughout the inhomogeneous sample).

A plot of local estimation of $\sqrt{\lambda_{\text{in-plane}}\lambda_{\text{through-plane}}}$ on the y axis (at the local time positions) vs $d_{p,\text{radial}}$ on the x axis (at the local time positions). However, as we are interested in the true depth position (normal direction from the plane of the hot disk sensor), $d_{p,\text{axial}}$ on the x-axis can be replaced with

$$d_{p,\text{axial}} = \frac{1}{\sqrt{AR}} \cdot d_{p,\text{radial}}. \quad (3)$$

In addition, on the y-axis, we can, instead, plot both the estimated local in-plane thermal conductivity,

$$\lambda_{\text{in-plane}} = \sqrt{AR} \cdot \sqrt{\lambda_{\text{in-plane}}\lambda_{\text{through-plane}}}, \quad (4)$$

and the estimated local through-plane thermal conductivity,

$$\lambda_{\text{through-plane}} = \frac{1}{\sqrt{AR}} \cdot \sqrt{\lambda_{\text{in-plane}}\lambda_{\text{through-plane}}}. \quad (5)$$

III. EXPERIMENTAL

A. Sample preparation

Two anisotropic samples were chosen to test the suggested computational method: a stack of printing paper and a stack of high temperature mica sheets with corresponding thicknesses of 0.13 and 0.50 mm, respectively. The parameters of the samples are presented in Table I.

In order to test the computational scheme in Sec. II, artificial defects were introduced inside the stack samples at certain depth

TABLE I. Parameters of the samples in the current work.

	$\lambda_{\text{through-plane}}$ (W/mK)	$\lambda_{\text{in-plane}}$ (W/mK)	$(\rho c_p)_{\text{true}}$ (MJ/m ³ K)	$(\rho c_p)_{\text{false}}$ (MJ/m ³ K)	\sqrt{AR}
Paper stack	0.079	0.464	0.945	0.42	2.25
Mica stack	0.129	2.466	1.79	0.41	4.37

TABLE II. Defects and their depth position in the sample of the current work.

Sample	Defect					
	Cu			Styrofoam		
Paper stack	At 1 mm	At 1.5 mm	At 2 mm
Mica stack	At 1 mm	At 1.5 mm	At 2 mm	At 1 mm	At 1.5 mm	...

positions in the normal direction from the plane of the hot disk sensor (Fig. 6). Two types of defects were introduced: either a thin layer of low thermal conductivity (Styrofoam, 5 mm thick) material or, alternatively, a thin layer of a high-thermal conductivity material (copper, 0.2 mm thick). The transient recordings of the samples with these defects placed at different depth positions were made. The different types of defects and their corresponding depth positions are summarized in Table II.

B. Measurement apparatus

All tests were performed using the transient plane source method, utilizing a TPS 3500 apparatus (produced by Hot Disk AB, Sweden) and a congenial hot disk Kapton sensor 5501 of 12.8 mm diameter.

First, the parameter $(\rho c_p)_{false}$ value was obtained using the Standard (isotropic) hot disk module.^{6,11} In accordance with Gustavsson and Gustafsson,¹² assuming an isotropic sample, the estimated thermal conductivity renders the geometric average thermal conductivity in the radial and normal directions, while the estimated thermal diffusivity represents the thermal diffusivity in the radial (in-plane) direction, i.e., Eq. (1) can be immediately applied.

Second, the parameter $(\rho c_p)_{true}$ value was estimated from the density (measured by the Archimedes method) of the corresponding stack and the tabular heat capacity per unit mass of paper and mica.

Utilizing Eq. (2), the anisotropy ratio of the material, AR, could be immediately determined.

The function of the thermal conductivity vs depth profile was acquired with the Structural Probe module based on a computational scheme outline developed by Sizov *et al.*,⁷ modified by inserting the false $(\rho c_p)_{false}$ as specific heat input and re-scaling the output probing depth according to Eq. (3) while computing the normal-direction thermal conductivity according to Eq. (5). Total measurement test times of 10–80 s were applied, with a total average temperature increase of the sensor between 3 and 5 K. The temperature responses of all samples are plotted in Figs. 3 and 4. In order to optimize accuracy and sensitivity for these tests, a double-sided symmetric setup was used—i.e., the hot disk sensor was sandwiched between identical sample pieces. Finally, a weight of 1.5 kg was applied in order to control the mounting pressure.

IV. RESULTS

Figures 1 and 2 display the outcomes of using thermal conductivity profiling to investigate defect mapping. To serve as a benchmark for detecting such defects, the mica and paper stacks, without any defects inserted, underwent analysis using the standard hot disk anisotropy method. The numerical value of this benchmark is indicated by the black constant line in the figures and is also presented in Table I.

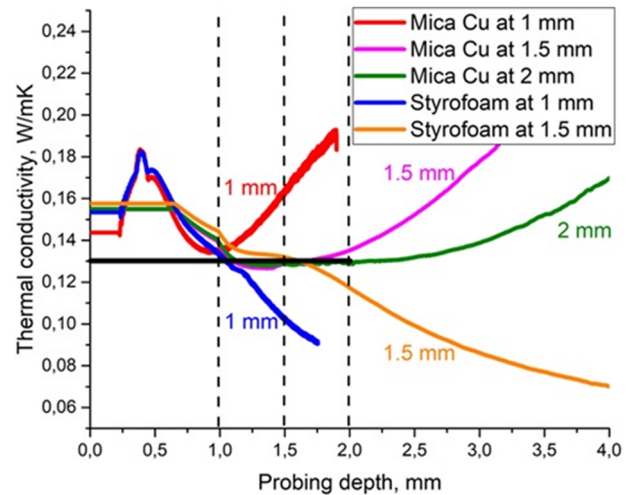


FIG. 1. Thermal conductivity in the normal direction vs depth profile of the mica stack with defects at different locations. The constant black line represents the $\lambda_{through-plane}$ obtained using the anisotropic method.¹²

The suggested new computations improve the depth position of the defects, as can be observed in Fig. 5 in Appendix B. Applying the original approach described in Sizov *et al.*⁷ [using $(\rho c_p)_{false}$], the thermal conductivity curve starts deviating at 3.5 mm, indicating the presence of a local inhomogeneity (defect) at this depth. However, the new approach recalculates the thermal conductivity and probing depth through-plane so that the thermal conductivity function deviates at a position of ~1.5 mm. This position of the defect is in line with the real position of the defect in the experimental setup.

The estimated normal-direction thermal conductivity function could differ slightly on depths shallower than the location of a defect. There could be a couple of reasons for this shift. One

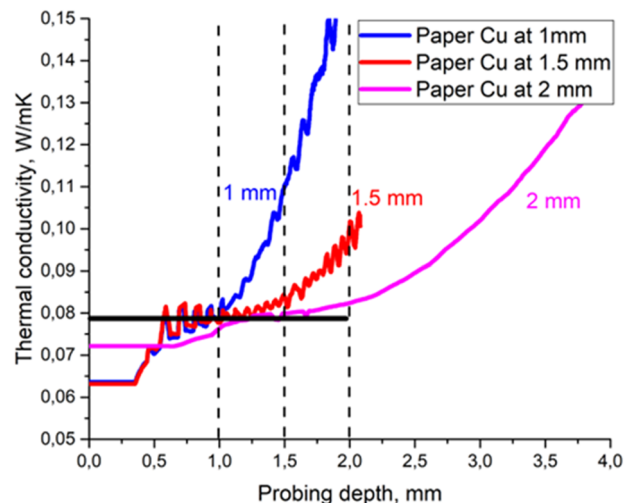


FIG. 2. Thermal conductivity in the normal direction vs depth profile of the paper stack with defects at different locations. The constant black line represents the $\lambda_{through-plane}$ obtained using the anisotropic method.¹²

24 July 2023 11:38:50

possible reason is the impact of modified thermal contact resistances between the stack sheet layers when the sample is remounted to include the different defects. It is worth noting that when defects are added to the mica stack, the employed computational routine generates a thermal conductivity value that is somewhat overestimated for the depth positions that are shallower than the copper or Styrofoam defects. Conversely, for the paper stack with defects, the computational routine produces a thermal conductivity value that is somewhat underestimated for the depth positions that are shallower than the copper or Styrofoam defects.

An important factor that could lead to deviation, particularly regarding the mica stack, is that the transient plane source technique typically requires heat flow across about ten layers to behave like a “continuum.” However, since the mica sheets are ~ 0.50 mm thick, this is not the case. As a result, for the layers closest to the hot disk sensor, the discrete influence of individual layers and contact resistances could significantly contribute to the overestimation of the local-position thermal conductivity. Nevertheless, the inhomogeneity computations, as shown in Fig. 1, indicate that the overestimation effect is clearly present only when the first two layers of mica are penetrated. At around 1 mm of probing depth, the estimated normal-direction thermal conductivity value matches the corresponding normal-direction anisotropy result for the homogeneous stack. For the paper stack, 0.13 mm thick, with introduced defects, the normal-direction thermal conductivity reaches the corresponding normal-direction thermal conductivity estimated by the anisotropy method somewhere between 0.5 and 1.0 mm probing depth.

V. DISCUSSION

The presence of underestimated or overestimated thermal conductivity values at the beginning of the graphs, i.e., at shallower depths, has a direct influence on the following calculation of the probing depth for greater depth positions. Hence, for the paper stack example, where the normal-direction thermal conductivity is underestimated at the beginning of the graph, the estimated position of the defect is computed to be located at a shallower depth as compared to the experimental setup. In contrast, for the mica stack example, where the thermal conductivity variation is overestimated at the beginning of the graph, the estimated position of the location of the depth is computed to be located at a deeper depth as compared to that of the experimental setup.

When the heat propagation reaches an inhomogeneous matter, the sensor records this as a slight temperature disturbance. This affects the calculation of thermal conductivity vs depth position. Similarly to what was found in the original publication,⁷ the estimated thermal conductivity at the inhomogeneity position will here show indications of inhomogeneity but will strongly underestimate the change in local thermal conductivity.

For instance, when heat propagation reaches a copper defect (with a thermal conductivity of ~ 400 W/mK), the thermal conductivity vs depth deviates toward a higher thermal conductivity value—while far short of the thermal conductivity of the Cu sheet (~ 400 W/mK). As found in the original publication,⁷ the deviation toward a different value will gradually decrease when the inhomogeneity position is placed at greater and greater depths—due to a significantly reduced measurement sensitivity with increasing probing depths.

A similar observation is made where a lower thermal conductivity value is recorded at the depth position of the Styrofoam material (~ 0.035 W/mK). However, it should be noted that the estimated thermal conductivity does not drop to the thermal conductivity value of the Styrofoam material.

In summary, it appears that the suggested calculation procedure allows for a non-destructive capability of tracking the depth position of a defect and provides some indication as to whether this defect is lower- or higher-conducting in nature. However, it should be remembered that any initial deviations located at the shallower depths of the thermal conductivity vs depth position graphs may offset the entire following depth positioning of deeper defects.

VI. POSSIBLE APPLICATIONS

The suggested method may be applied in situations where it is of interest to detect or track inhomogeneities in the normal direction of a sample in a non-destructive manner. The presence of anisotropy (via texture) is often a real effect normally not accounted for in thermal conductivity testing. Accounting for an underlying anisotropy is suggested to make more accurate depth-positioning possible, as more or less most solid materials show the presence of anisotropy in the thermal conductivity. The application of a heat pulse in the probe results in a maximum temperature increase of the double-spiral of perhaps 3–4 K, which, accounting for the presence of the Kapton layer and possible interfacial thermal contact resistance between the surface of the probe and sample surface, results in a maximum temperature increase of the sample surface of perhaps 1–2 K or similar—a temperature disturbance that is believed not to influence most solid, inert sample materials. Temperature vs time recordings can be made highly reproducible and sensitive, allowing, for instance, for a rough monitoring of a diffusion- or cell-change-spreading process after applying a skin lotion or a skin cream on living human skin if recorded at the same position at defined time intervals.

A comparison between skin tumor and thermal conductivity variation adjacent to a tumor was reported in Ref. 7, utilizing the original structural probing computational scheme, for a non-destructive measurement on live skin. The presented computational scheme is expected to enhance the accuracy of estimating the thickness of the skin tumor, including substructure deviations, due to the inherently anisotropic nature of the skin's texture. It is anticipated that further studies can be conducted utilizing the proposed technique, such as monitoring the long-term healing process of a burn wound.¹³

AUTHOR DECLARATIONS

Conflict of Interest

The authors have no conflicts to disclose.

Author Contributions

A. Sizov: Data curation (lead); Formal analysis (lead); Investigation (lead); Software (lead); Validation (lead); Visualization (lead); Writing – original draft (equal). **B. Mihiretie:** Conceptualization (supporting); Investigation (supporting); Software (supporting); Visualization (equal); Writing – original draft (supporting); Writing –

review & editing (equal). **Y. Ma:** Conceptualization (supporting); Software (supporting); Supervision (supporting); Writing – review & editing (supporting). **S. E. Gustafsson:** Conceptualization (supporting); Methodology (supporting); Resources (equal); Supervision (supporting); Writing – original draft (supporting). **M. Gustavsson:** Conceptualization (equal); Formal analysis (equal); Project administration (equal); Supervision (equal); Writing – review & editing (equal).

DATA AVAILABILITY

The data that support the findings of this study are available from the corresponding author upon reasonable request.

APPENDIX A: TEMPERATURE RESPONSE VS TIME

The temperature response vs time for Mica and paper stacks with defects at different positions are depicted in Fig. 3 and Fig. 4, respectively.

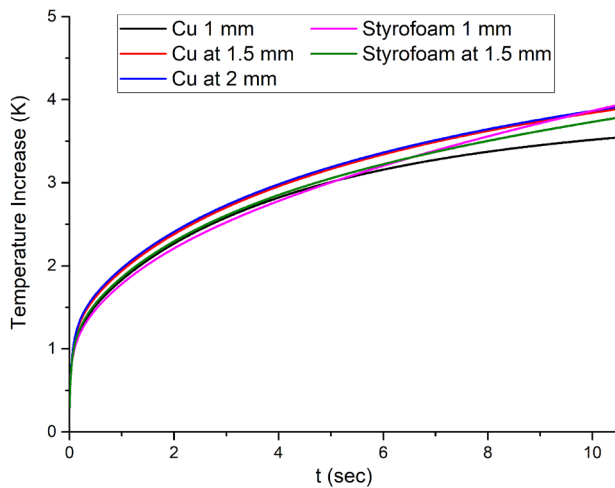


FIG. 3. Thermal response of mica stacks with defects at different depths.

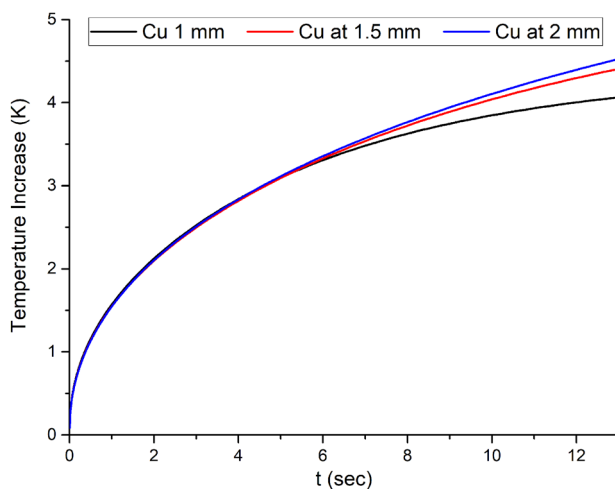


FIG. 4. Thermal response of paper stacks with defects at different depths.

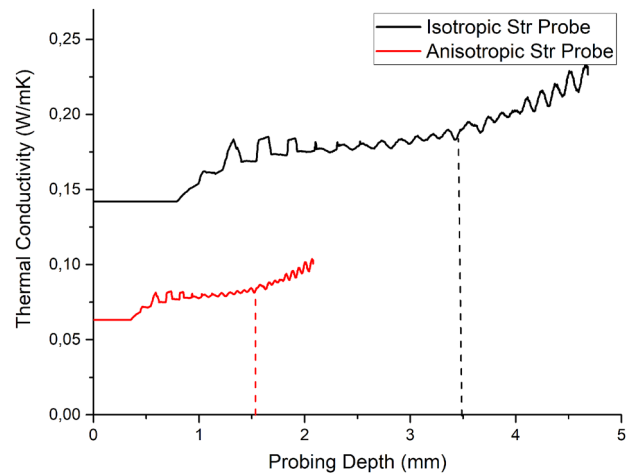


FIG. 5. Thermal conductivity vs probing depth, acquired using the original method with $(\rho c_p)_{false}$ and the new approach for comparison.

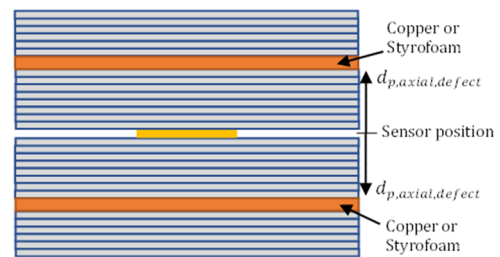


FIG. 6. Schematic measurement setup.

APPENDIX B: IMPROVEMENTS OF DEPTH POSITION ESTIMATIONS WITH THE NEW COMPUTATIONAL SCHEME

Thermal conductivity vs probing depth functions, acquired using the original method and the new approach for comparison, are depicted in Fig. 5.

APPENDIX C: SCHEMATIC MEASUREMENT SETUP

The schematic measurement setup (side view cross-section) is depicted in Fig. 6.

REFERENCES

- ¹S. E. Gustafsson, “Transient plane source techniques for thermal conductivity and thermal diffusivity measurements of solids materials,” *Rev. Sci. Instrum.* **62**, 797–804 (1991).
- ²Y. He, “Rapid thermal conductivity measurement with a hot disk sensor: Part 1. Theoretical considerations,” *Thermochim. Acta* **436**, 122–129 (2005).
- ³A. L. Cottrill, A. T. Liu, Y. Kunai *et al.*, “Ultra-high thermal effusivity materials for resonant ambient thermal energy harvesting,” *Nat. Commun.* **9**, 664 (2018).
- ⁴K. Maeda, Y. Tsunetsugu, K. Miyamoto, and T. Shibusawa, “Thermal properties of wood measured by the hot-disk method: Comparison with thermal properties measured by the steady-state method,” *J. Wood Sci.* **67**, 20 (2021).

24 July 2023 11:38:50

- ⁵V. Bohac, M. Gustavsson, L. Kubicar, and V. Vretenar, “Measurements of building materials by transient methods,” in *Thermophysics 2003* (Kočovce, Slovakia, 2003), pp. 53–66.
- ⁶ISO 22007-2, Plastics—Determination of thermal conductivity and thermal diffusivity—Part 2: Transient plane heat source (hot disc) method, 2015.
- ⁷A. Sizov, D. Cederkrantz, L. Salmi, A. Rosén, L. Jacobson, S. E. Gustafsson, and M. Gustavsson, “Thermal conductivity versus depth profiling of inhomogeneous materials using hot disc technique,” *Rev. Sci. Instrum.* **87**, 074901 (2016).
- ⁸M. Gustavsson and S. E. Gustafsson, “Thermal conductivity as an indicator of fat content in milk,” *Thermochim. Acta* **442**, 1–5 (2006).
- ⁹B. M. Mihiretie, D. Cederkrantz, M. Sundin, A. Rosén, H. Otterberg, Å. Hinton, B. Berg, and M. Karlsteen, “Thermal depth profiling of materials for defect detection using hot disk technique,” *AIP Adv.* **6**, 085217 (2016).
- ¹⁰V. Bohac, M. K. Gustavsson, L. Kubicar, and S. E. Gustafsson, “Parameter estimations for measurements of thermal transport properties with the hot disk thermal constant analyzer,” *Rev. Sci. Instrum.* **71**, 2452 (2000).
- ¹¹Instruction manual, hot disk thermal constants analyser, Hot Disk AB, Johanneberg Science Park, Sweden, 2019.
- ¹²M. Gustavsson and S. Gustafsson, “On the use of transient plane source sensors for studying materials with direction dependent properties,” in *Thermal Conductivity 26: Thermal Expansion 14: Joint Conferences* (DEStech Publications, Inc., Lancaster, PA), p. 367.
- ¹³S. R. Krishnan, C.-J. Su, Z. Xie *et al.*, “Wireless, battery-free epidermal electronics for continuous, quantitative, multimodal thermal characterization of skin,” *Small* **14**, 1803192 (2018).